Is chloroplast size optimal for photosynthetic efficiency?

Katarzyna Głowacka[1,2,3] iD, Johannes Kromdijk[1,4] iD, Coralie E. Salesse-Smith[1] iD, Cailin Smith[2,5] iD, Steven M. Driever[1,6] iD and Stephen P. Long[1,7] iD

[1]Carl R. Woese Institute for Genomic Biology, University of Illinois at Urbana-Champaign, 1206 West Gregory Drive, Urbana, IL 61801, USA; [2]Department of Biochemistry and Center for Plant Science Innovation, University of Nebraska-Lincoln, 1901 Vine Street, Lincoln, NE 68588, USA; [3]Institute of Plant Genetics, Polish Academy of Sciences, Strzeszynska 34, Poznań, 60-479, Poland; [4]Department of Plant Sciences, University of Cambridge, Downing Street, Cambridge, CB2 3EA, UK; [5]Goshen College, 1700 South Main Street, Goshen, IN 46526, USA; [6]Centre for Crop Systems Analysis, Wageningen University, Bornsesteeg 48, Wageningen, 6708PE, the Netherlands; [7]Departments of Plant Biology and of Crop Sciences, University of Illinois, 505 South Goodwin Avenue, Urbana, IL 61801, USA

Author for correspondence:
Katarzyna Głowacka
Email: *kglowacka2@unl.edu*

Summary

- Improving photosynthetic efficiency has recently emerged as a promising way to increase crop production in a sustainable manner. While chloroplast size may affect photosynthetic efficiency in several ways, we aimed to explore whether chloroplast size manipulation can be a viable approach to improving photosynthetic performance.
- Several tobacco (*Nicotiana tabacum*) lines with contrasting chloroplast sizes were generated via manipulation of chloroplast division genes to assess photosynthetic performance under steady-state and fluctuating light. A selection of lines was included in a field trial to explore productivity.
- Lines with enlarged chloroplasts underperformed in most of the measured traits. Lines with smaller and more numerous chloroplasts showed a similar efficiency compared with wild-type (WT) tobacco. Chloroplast size only weakly affected light absorptance and light profiles within the leaf. Increasing chloroplast size decreased mesophyll conductance (g_m) but decreased chloroplast size did not increase g_m. Increasing chloroplast size reduced chloroplast movements and enhanced non-photochemical quenching. The chloroplast smaller than WT appeared to be no better than WT for photosynthetic efficiency and productivity under field conditions.
- The results indicate that chloroplast size manipulations are therefore unlikely to lead to higher photosynthetic efficiency or growth.

Introduction

The demand for global food production is estimated to increase between 50% and 100% by 2050 due to predicted growth in global population and increase in calorie demand associated with growing incomes (Tilman *et al.*, 2011; Alexandratos & Bruinsma, 2012; FAO *et al.*, 2020). However, the annual increase in yield of most staple crops is not rising at a sufficient pace to double global production by 2050 (Ray *et al.*, 2013). In addition, future food security will also require mitigation of yield losses due to negative environmental factors, such as drought and heat (Le Quéré *et al.*, 2009; Lobell *et al.*, 2014; Dalin *et al.*, 2017; Kim *et al.*, 2017), and new directions for research and policy have to be undertaken to help meet both sustainability and production goals (Hunter *et al.*, 2017).

Improving photosynthetic efficiency has recently emerged as a promising way to increase crop production in a sustainable manner (Rosenthal *et al.*, 2011; Long *et al.*, 2015; Kromdijk *et al.*, 2016; Köhler *et al.*, 2017; Bailey-Serres *et al.*, 2019; Ermakova *et al.*, 2019; Simkin *et al.*, 2019; South *et al.*, 2019; López-

Calcagno *et al.*, 2020; Yoon *et al.*, 2020; De Souza *et al.*, 2022). In the current study, we explored whether photosynthetic efficiency could be improved by modifying chloroplast size. Chloroplast size may affect photosynthetic efficiency in several ways. First of all, smaller chloroplasts have a proportionally greater surface area relative to their volume than large chloroplasts, which could be expected to improve CO_2 diffusion. As a result, chloroplast size could affect the CO_2 conductance from intercellular air-space to chloroplast stroma (Weise *et al.*, 2015; Xiong *et al.*, 2017), which is termed mesophyll conductance (g_m). Lower g_m is associated with larger chloroplasts (Weise *et al.*, 2015), but the opposite scenario, increased g_m due to reduction in chloroplast size, has not yet been assessed. Second, chloroplast size may also affect leaf light absorption characteristics. Light attenuation is an important component of photosynthetic efficiency, and theoretically, a uniform distribution of light across all chloroplasts is optimal for photosynthetic efficiency because of the hyperbolic shape of the photosynthetic light response (Xiao *et al.*, 2023). Lower transmission was observed for leaves of chloroplast mutant lines with large chloroplasts (Jeong *et al.*, 2002; Königer *et al.*,

2008), but it is currently unclear to what extent this was caused specifically by size alterations or instead by concomitant reductions in chlorophyll content and chl$a$: chl$b$ ratio. Finally, chloroplast size is also important for the ability to undergo chloroplast movements. The movement toward weak light and movement away from strong light contribute to photosynthetic efficiency via maximization of light interception and protection from photodamage, respectively (Wada *et al.*, 2003). Several studies have shown that large chloroplasts have a reduced ability to undergo photorelocation, affecting the time required to adjust to light fluctuations (Jeong *et al.*, 2002; Königer *et al.*, 2008; Dutta *et al.*, 2017). However, the effect of reducing chloroplast size on the photorelocation response has received little attention (Dutta *et al.*, 2017).

The molecular mechanism of chloroplast division is well known. The filamenting temperature-sensitive Z (FtsZ) 1 and FtsZ2 proteins initiate division by the formation of a ring in the stroma. The FtsZ ring is stabilized by the Accumulation and Replication of Chloroplasts 6 (ARC6) protein that spans across the inner chloroplast envelope. Through the interaction with ARC6 and mediation of paralog of ARC6, the outer envelope-spanning proteins of Plastid Division (PDV) 1 and PDV2 are recruited to the division side. Then, the PDVs recruit the dynamin-related protein so that the entire division complex is formed and fission of the chloroplast can occur. Distortion of the ratio of FtsZ1 : FtsZ2 protein results in a smaller population of enlarged chloroplasts (e.g. Osteryoung *et al.*, 1998; Jeong *et al.*, 2002; Dutta *et al.*, 2017), while overexpression of either PDV1 or PDV2 leads to more numerous but smaller chloroplasts, with the effect being exacerbated when both are jointly overexpressed (Okazaki *et al.*, 2009).

Here, we aimed to explore whether chloroplast size manipulation can be a way to improve photosynthetic performance. To do so, we generated several tobacco (*Nicotiana tabacum*) lines with contrasting chloroplast sizes via manipulation of the chloroplast division proteins FtsZ and PDV. These lines were used to assess photosynthetic performance under steady-state and fluctuating light. Furthermore, a selection of lines was included in a field trial to explore productivity. Altogether, the results indicate that altering chloroplast size may not have much potential to improve photosynthetic efficiency, with lines with enlarged chloroplasts most clearly underperforming in most of the measured traits. Lines with smaller, more numerous chloroplasts generally showed a similar efficiency compared with wild-type (WT) tobacco; however, none of the hypothesized benefits were observed and productivity was negatively impacted.

Materials and Methods

Plant material and transformation

Three binary plasmids were used in transformation, pATFTSZ1, pSLPDV1, and pSLPVD2, containing the coding sequence of *Arabidopsis thaliana* filamenting temperature-sensitive Z 1 gene (*AtFtsZ1*), tomato (*Solanum lycopersicum*) plastid division protein 1 (*SlPDV1*), and the tomato plastid division protein 2 (*SlPDV2*),

respectively (Supporting Information Fig. S1). The chloroplast division genes were driven by *A. thaliana* Ribulose-1,5-bisphosphate carboxylase/oxygenase (Rubisco) small subunit 1b promoter. All plasmids were assembled using the golden-gate system (Engler *et al.*, 2009). *Nicotiana tabacum* L. cv Petit Havana carrying TMV resistance (NN) was transformed using *Agrobacterium*-mediated transformation (Clemente, 2006). Between 25 and 29 independent events were generated per construct. T-DNA copy number for each event was assessed using digital droplet PCR (ddPCR; Głowacka *et al.*, 2016; primer sequences in Table S1). For each construct, homozygous T2 progeny were obtained for 5–8 independent events with a single T-DNA insertion site, as well as one line with two T-DNA insertion sites (PDV2-1). Results shown in this paper are either for homozygous offspring of T2 generation or F1 progeny of the cross between SlPDV2 and SlPDV1 lines. Corresponding WT seeds collected from WT which was grown alongside and under the same conditions as the transformants were used as the control in all experiments.

Plant propagation in glasshouse or growth chamber

Seeds were germinated on growing medium (LC1 Sunshine mix; Sun Gro Horticulture, Agawam, MA, USA) in a controlled environment walk-in growth chamber (Environmental Growth Chambers, Chagrin Falls, OH, USA) with 12 h photoperiod, 18°C : 20°C (night : day) and light intensity of 150 μmol m^{-2} s^{-1}. Five days after germination, seedlings were transplanted to 9 × 4 potting trays (3600 series; Hummert International, Earth City, MO, USA) and grown until two true leaves had emerged in glasshouse or growth chamber (PGC20; Conviron, Winnipeg, MB, Canada) with 16 h photoperiod and air temperature controlled at 20°C : 25°C (night : day) and light controlled at 500 μmol m^{-2} s^{-1}. At the two-leaf stage, seedlings were transplanted to 3.8 l pots (400C; Hummert International) filled with growing medium (LC1 Sunshine mix; Sun Gro Horticulture) supplemented with 10 g granulated fertilizer per pot (Osmocote Plus 15/9/12; The Scotts Co. LLC, Marysville, OH, USA). Pots were randomized in position and spaced 30 cm apart on the glasshouse table or inside the growth chamber. Plants were watered, and plant positions were changed randomly every other day until the fifth leaf was fully expanded.

Gene expression

Lines were grown in three batches with corresponding WT included in each batch. A total of 2.9 cm^2 from the most recent fully expanded leaf were sampled per plant *c.* 2 h after the start of the photoperiod. The mRNA extracted using NucleoSpin RNA/Protein kit (REF740933; Macherey-Nagel GmbH & Co. KG, Düren, Germany) was treated by DNase (Turbo DNA-free kit, AM1907; Thermo Fisher Scientific, Waltham, MA, USA) before being transcribed to cDNA using Superscript III First-Strand Synthesis System for RT-PCR (18080-051; Thermo Fisher Scientific). RT-qPCR was used to quantify expression levels of the transgenes *AtFTSZ1*, *SlPDV1*, and *SlPDV2*, and the corresponding native genes *NtFTSZ1*, *NtPDV1*, and *NtPDV2* relative

to actin (*NtActin*) and elongation factor-1α (*NtEF-1α*; primer sequences in Table S1).

Chloroplast morphology

Before collection of tissue for microscopy, plants from controlled environment were incubated in weak laboratory light for *c.* 20 h to destarch chloroplasts. For field-grown plants, leaves were covered in aluminum foil sleeves the evening before sampling *c.* 2 h after sunrise the next day. Fragments of the second interveinal segment were collected from fully expanded leaves, the epidermal layer was removed from the abaxial side, and samples were fixed for 1 h in the dark in 3.5% glutaraldehyde (16 000; Electron Microscopy Science (EMS), Hatfield, PA, USA). The fixed tissue was softened in 0.1 M Na$_2$EDTA pH 9 (E6635; Sigma) for 20 min at 50°C with shaking (modified from Okazaki *et al.*, 2009) and stored at 4°C until imaged. The suspended protoplasts were mounted on a slide, and chloroplast features were analyzed using a confocal microscope with Nomarski optics (LSM 710; AxioObserver using the C-Apchromat 40×/1.20 W Korr M27 objective; Zeiss). A practical decision was made to focus the chloroplast morphological analysis exclusively on palisade mesophyll cells, since these appeared to have more uniform chloroplast morphology than spongy mesophyll cells. Image analysis was performed in IMAGEJ (1.53e; NIH, Rockville, MD, USA) to obtain the diameter at the major (LD) and minor (SD) axis and estimate the chloroplast number per cell. The eccentricity (*e*), as a measure of the deviation from circularity, was calculated according to Eqn 1:

$$e = \sqrt{1 - \frac{\left(\frac{SD}{2}\right)^2}{\left(\frac{LD}{2}\right)^2}} \qquad \text{Eqn 1}$$

The spheroid volume (*V*$_s$) and area (*A*$_s$) were calculated according to Eqns 2, 3, respectively:

$$V_s = \left(\frac{LD}{2}\right)^2 \frac{SD}{2} \qquad \text{Eqn 2}$$

$$A_s = 2\pi \left(\frac{LD}{2}\right)^2 + \pi \frac{\left(\frac{SD}{2}\right)^2}{e} \log\left(\frac{1+e}{1-e}\right) \qquad \text{Eqn 3}$$

Based on the chloroplast morphology, line FTSZ1-16 was selected to evaluate the effect of large chloroplasts and lines PDV1-9 and PDV2-17 were selected to evaluate the effect of small chloroplasts on photosynthetic efficiency and growth. To obtain a further reduction in chloroplast size, the F1 generation of a cross between PDV2-9 and PDV1-9 was also included for further analysis.

Chloroplast movement

Transition of chloroplasts from the accumulation at the top of the cell in the low light to avoidance position on the vertical walls in high light and vice versa were estimated from time series of transmittance in the wavelength between 600 and 650 nm. To stimulate chloroplast movement, blue-light illumination with different intensity was applied, which is shown to be crucial in the activation of chloroplast movement (Banaś *et al.*, 2012). For the detailed protocol, see Methods S1.

Leaf anatomy and morphology

Leaf tissue was fixed in a mixture of glutaraldehyde and paraformaldehyde, dehydrated through a graded ethanol series, and then imbedded in epoxy mixture for sectioning at 0.35 μm. Sections were stained with toluidine blue and basic fuchsin and viewed with an Olympus BH2 microscope (Olympus, Center Valley, PA, USA). For details of the protocol, see Methods S2. IMAGEJ software was used to measure in the light micrographs the lengths of wall exposed to intercellular airspace of mesophyll cells (*L*$_{mes}$) and length of the chloroplasts touching the plasma membrane appressed to the intercellular air space (*L*$_c$). Surface areas exposed to intercellular airspace of mesophyll (*S*$_{mes}$) and abutted by chloroplasts (*S*$_c$) were calculated using the following equations (Evans *et al.*, 1994):

$$S_{mes} = \frac{L_{mes}}{W} \gamma \qquad \text{Eqn 4}$$

where *W* is the width of each section and *γ* is the curvature correction factor of 1.34.

$$S_c = \frac{L_c}{L_{mes}} S_{mes} \qquad \text{Eqn 5}$$

Sections of 5 × 10 mm of the second interveinal segment of the fully expanded leaf were collected from glasshouse-grown plants and embedded in 1% ultrapure agarose (16 500; Fisher, Waltham, MA, USA) using a mold (50-930-532; Fisher). The agarose block was cut in half and placed with the cut-edge-down onto a fluorodish (50-823-005; Fisher) into a drop of water. Using confocal microscopy (LSM710; Zeiss) equipped with EC-Plan_Neoflor 10× objective, the leaf section was illuminated with the excitation wavelength of 633 nm with the resulting chlorophyll fluorescence detected at 654 nm. Image analysis was performed in IMAGEJ to obtain the diameter at the major and minor axis of the palisade mesophyll cells, the number of palisade mesophyll cells, and the width of the leaf.

Quantification of photosynthesis-related pigments

Photosynthesis-related pigments were extracted from leaf tissue using 100% methanol. The absorbance at 470, 652, and 665 nm of the extract was assessed spectrophotometrically. Concentrations of chl*a*, chl*b* and total carotenoids were determined from the measured absorptions following the equations of Lichtenthaler (1987). For the detailed protocol, see Methods S3.

Photosynthetic gas exchange and PAM fluorescence

Gas exchange measurements were performed using an open gas exchange system equipped with a temperature-controlled leaf

chamber incorporating an integrated modulated fluorometer and LED illumination (LI6400XT and LI6400-40; LI-COR, Lincoln, NE, USA). Pulse amplitude-modulated chlorophyll fluorescence (PAM) measurements used the multiphase flash routine (Loriaux *et al.*, 2013) in parallel with gas exchange measurements at a range of light intensities to determine the light response of net CO_2 assimilation (A_n), linear electron transport (J), and nonphotochemical quenching (NPQ). The environmental conditions in the cuvette were maintained as follows: block temperature at 25°C, (CO_2) at 400 µmol mol^{-1} and leaf-to-air water VPD between 1.1 and 1.4 kPa. Leaves were dark-adapted overnight (only the controlled condition-grown plants) and in the leaf cuvette for an additional 20 min, after which minimal (F_o) and maximal fluorescence (F_m) were measured to determine maximal efficiency of whole-chain electron transport (F_v/F_m; Genty *et al.*, 1989):

$$F_v/F_m = (F_m - F_o)/F_m \qquad \text{Eqn 6}$$

Subsequently, light-response curves were measured using either 100% red LEDs or 90% red and 10% blue LEDs by slowly increasing from 0 to 50, 80, 110, 140, 170, 200, 300, 400, 500, 600, 800, 1000, 1500, and 2000 µmol m^{-2} s^{-1}. Both curves were measured on the opposite sides of the midrib on the same leaf. For field-grown plants, the environmental conditions in the cuvette were maintained as followed: block temperature at 30°C, (CO_2) at 400 µmol mol^{-1} and leaf-to-air water VPD below 1.5 kPa. After steady-state gas exchange was reached at 2000 µmol m^{-2} s^{-1} (90%/10% red/blue), light intensity was varied from 2000 to 1500, 1000, 800, 600, 400, 200, 170, 140, 110, 80, and 50 µmol m^{-2} s^{-1}. In all cases, when steady state was reached gas exchange parameters were logged and F' and F'_m were measured to estimate PSII operating efficiency (ΦPSII) according to Eqn 7 (Genty *et al.*, 1989) and in case of glasshouse-grown plants also NPQ Eqn 8 (Bilger & Björkman, 1994)

$$\Phi\text{PSII} = \frac{(F'_m - F')}{F'_m} \qquad \text{Eqn 7}$$

$$\text{NPQ} = \frac{F_m}{F'_m} - 1 \qquad \text{Eqn 8}$$

Leaf absorptance of incident irradiance (α_l) was measured as close as possible to the spot where gas exchange analysis was performed, using a LI1800 integrating sphere connected to a USB-2000 spectrometer. Rates of J were determined according to Eqn 9.

$$J = \alpha_l \times \Phi\text{PSII} \times PFD \times 0.5 \qquad \text{Eqn 9}$$

where PFD is the incident photon flux density (µmol m^{-2} s^{-1}).

Quantum efficiency of linear electron transport (ΦPSII$_{max}$) and quantum efficiency of leaf net CO_2 assimilation (ΦCO_{2max}) were derived from the initial slope of the light response of J and A_n, respectively. Mitochondrial respiration rate in the light (R_l) was the y-axis intercept of the light response of A_n. J_{max} and A_{sat}

were obtained by fitting a nonrectangular hyperbola to the light-response curves of J and A_n, respectively (Long & Bernacchi, 2003). The light responses of NPQ were fitted to a sigmoidal Hill function (Eqn 10; Kromdijk *et al.*, 2019) by fitting the asymptote of the response (NPQ$_{max}$), the y-axis intercept; (NPQ$_0$), the PFD in which NPQ reaches half of the maximum values (K$_{NPQ}$) and the Hill coefficient (nNPQ).

$$\text{NPQ} = \frac{(\text{NPQ}_{max} - \text{NPQ}_0)}{\left(\frac{\text{K}_{NPQ}}{\text{PFD}}\right)^{n\text{NPQ}} + 1} + \text{NPQ}_0 \qquad \text{Eqn 10}$$

In addition to the steady-state light-response curves, a dynamic light-response curve (90% red and 10% blue LEDs) was reconstructed from a timed series of changes in light intensity. First, leaves were allowed to reach steady-state gas exchange at 2000 µmol m^{-2} s^{-1}. Then, light intensity was set to 14 decreasing values as in Kromdijk *et al.* (2016). Each step lasted 4 min and was preceded by 4 min of 2000 µmol m^{-2} s^{-1}. At each light intensity, the F' and F'_m and gas exchange parameters were determined after 60, 140, and 220 s. The values of these three measurements were averaged and used to reconstruct light-response curves analyzed as described previously.

To analyze the CO_2 response of A_n, leaves were clamped in the cuvette with block temperature controlled at 25°C (or 30°C for field-grown plants) and light intensity set to 2000 µmol m^{-2} s^{-1} (90% red and 10% blue LEDs). CO_2 concentration in the cuvette was set to 14 subsequent values 400, 300, 250, 200, 150, 100, 75, 400, 400, 600, 800, 1000, 1200, and 1500 µmol mol^{-1} and gas exchange parameters were logged when steady state was reached. The resulting gas exchange measurements were corrected for leaks between the cuvette and the surrounding atmosphere estimated from dark measurements of mitochondrial respiration (R_d) at contrasting CO_2 concentrations. A model for leaf photosynthesis (Farquhar *et al.*, 1980) with temperature corrections was fitted to the response of A_n to intercellular CO_2 concentration (C_i) to estimate the maximal carboxylation rate (V_{cmax}), maximal linear electron transport rate (J_{max}), and triose phosphate utilization rate (TPU) using the spreadsheet provided by Sharkey *et al.* (2007).

Carbon isotope discrimination ($\Delta^{13}C$) and estimation of g_m

Mesophyll conductance was derived from carbon isotope discrimination ($\Delta^{13}C$) during photosynthetic gas exchange. $\Delta^{13}C$ was determined as described before (Kromdijk *et al.*, 2020) with some small modifications. Leaves were clamped in the cuvette of an open gas exchange system with integrated multiphase flash fluorometer (LI6800; LI-COR). Light intensity was set to 2000 µmol m^{-2} s^{-1}, leaf temperature was controlled at 25°C, and CO_2 concentration in the cuvette was maintained at 400 µmol mol^{-1}. Measurements were performed at O_2 concentrations of 2 or 21%. CO_2 samples from reference line and cuvette air were obtained from the LI6800 exhaust ports using two parallel cryogenic trapping and purification lines under partial vacuum as described in Kromdijk *et al.* (2010). After A_n and
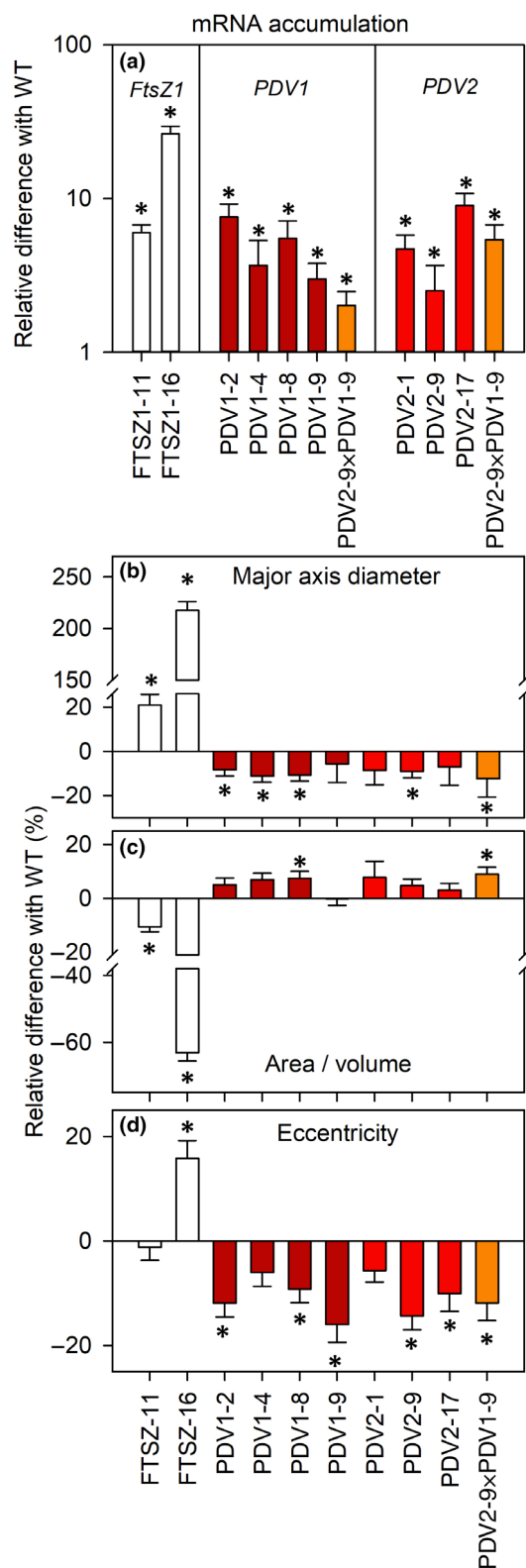
Fig. 1 Effect of ectopic expression of chloroplast division genes on transcript and chloroplast morphology in *Nicotiana tabacum* grown under glasshouse conditions. (a) The total accumulation of filamenting temperature-sensitive Z1 (*FtsZ1*), plastid division protein 1 (*PDV1*) and *PDV2* mRNA. (b) Size of chloroplasts estimated from the major axis diameter and shape estimated from (c) the ratio of chloroplast area to its volume and (d) eccentricity. The FTSZ1-11 and -16 lines express gene of *Arabidopsis thaliana FtsZ1*; PDV1-2, -4, -8, and -9 lines express tomato (*Solanum lycopersicum*) *PDV1*, PDV2-1, -9, and -17 lines express tomato gene of *PDV2*; PDV2-9 × PDV1-9 is F1 generation of a cross of PDV2-9 and PDV1-9 lines. In each panel, data are expressed as relative difference with the corresponding wild-type (WT). In panel (a) error bars indicate SE (*n* from 3 to 6 biological replicates); in panels (b–d) error bars indicate SE (*n* = 3 biological replicates with the exception of PDV2-1, WT corresponding to PDV2-1 and WT corresponding to FTSZ1-11 for which two biological replicates were analyzed; biological replicate for each line represents 200 chloroplasts with the exception of FTSZ1-16 line where each biological replicate represents from 40 to 52 chloroplasts and FTSZ1-11 for which each biological replicate represents from 181 to 200 chloroplasts). In all panels, asterisks indicate significant differences between transgenic lines and corresponding WT in Dunnett's two-way test: *P* ≤ 0.05. Data used to produce this figure are given in Datasets S1, S2.

spectrometer (SIRA series II; VG Isotech, modified by Provac Ltd, Crewe, UK). $\Delta^{13}C$ was derived from measured CO_2 mole fractions and isotope compositions in reference and cuvette air, according to Evans *et al.* (1986). From $\Delta^{13}C$ g_m was calculated using equations of Evans & Von Caemmerer (2013), using 29‰ for Rubisco fractionation factor *b* and 16.2‰ for photorespiratory fractionation factor *f*.

Estimation of light profiles within the leaf

Profiles of absorbed light within the leaf were measured using light-sheet microscopy, as in Slattery *et al.* (2016). To investigate the effect of reduction in internal scattering due to phase changes, water-infiltrated and unfiltered samples were used. The leaf sections were illuminated with the following excitation wavelengths: 405, 488, 561, and 638 nm, and the light absorption was determined from chlorophyll fluorescence. For the detailed protocol, see Methods S4.

Field experiment

The seeds of FTSZ1-16, PDV2-17, PDV2-9 × PDV1-9, and WT were sown in the glasshouse on 7 May 2018. Twenty-four-day-old seedlings were transplanted by hand to a field at the University of Illinois Energy Farm (40.11°N, 88.21°W). The experiment used a complete randomized block design with 12 blocks of 6 × 6 plants (Fig. S2). The field weather conditions are reported in Fig. S3. Photosynthesis measurements were performed 17 and 20 d after transplanting. Plants were harvested on July 7, 2018. For the detailed protocol, see Methods S5.

Statistical analysis

All statistical analyses were performed with SAS (v.9.4; SAS Institute Inc., Cary, NC, USA). Data were tested with the

stomatal conductance had reached steady state, samples of CO_2 were collected from reference and cuvette air for 5 min, while gas exchange parameters were logged. The carbon isotope composition of samples was analyzed on an isotope ratio mass

Table 1 Morphological and anatomical traits of chloroplast and leaf of growth-chamber-grown *Nicotiana tabacum* lines with modified chloroplast sizes and corresponding wild-type (WT).

Parameter	FTSZ1-16	WT	PDV1-9	PDV2-17	PDV2-9 × PVD1-9	*P*-value
Chloroplast morphological traits						
LD (µm)	21.1 ± 0.9*	6.66 ± 0.05	6.28 ± 0.07	6.20 ± 0.03	5.84 ± 0.11*	< **0.0001**
SD (µm)	13.9 ± 0.7*	4.94 ± 0.09	5.10 ± 0.04	4.89 ± 0.09	4.65 ± 0.05	< **0.0001**
SD/LD (−)	0.666 ± 0.007*	0.749 ± 0.010	0.820 ± 0.011*	0.797 ± 0.011*	0.803 ± 0.008*	< **0.0001**
Area (µm^2)	899 ± 80*	91.4 ± 1.7	83.5 ± 1.3	80.9 ± 0.9	72.5 ± 2.3*	< **0.0001**
Volume (µm^3)	3497 ± 520*	119 ± 4	109 ± 2	103 ± 2	88.1 ± 3.5*	< **0.0001**
Area/Volume (−)	0.294 ± 0.024*	0.798 ± 0.012	0.797 ± 0.005	0.823 ± 0.010	0.870 ± 0.013*	< **0.0001**
Eccentricity (−)	0.745 ± 0.017*	0.644 ± 0.014	0.541 ± 0.017*	0.579 ± 0.016*	0.567 ± 0.012*	< **0.0001**
Leaf morphological and anatomical traits						
Chloroplast number/Cell (−)	13.5 ± 0.6*	88.5 ± 13.4	94.8 ± 9.9	124.7 ± 4.9	93.3 ± 10.6	< **0.0001**
Cell LD (µm)	173 ± 35	146 ± 17	128 ± 7	153 ± 3	135 ± 6	0.48
Cell SD (µm)	32.2 ± 2.4	36.0 ± 3.5	35.5 ± 3.2	34.4 ± 1.1	30.8 ± 0.8	0.54
Cell number/100 µm (µm^{-1})	3.18 ± 0.21	3.07 ± 0.33	3.13 ± 0.15	3.03 ± 0.09	3.28 ± 0.16	0.89
L_{meas} (µm)	4390 ± 214	4469 ± 247	4868 ± 360	4284 ± 291	4241 ± 309	0.57
L_c (µm)	3998 ± 175	3894 ± 265	4402 ± 331	3795 ± 222	3840 ± 309	0.54
S_{mes} (m^2 m^{-2})	15.7 ± 0.8	16.0 ± 0.9	17.4 ± 1.3	15.3 ± 1.0	15.1 ± 1.1	0.57
S_c (m^2 m^{-2})	14.3 ± 0.6	13.9 ± 0.9	15.7 ± 1.2	13.6 ± 0.8	13.7 ± 1.1	0.54
S_c/S_{mes} (−)	0.910 ± 0.010	0.871 ± 0.022	0.904 ± 0.003	0.887 ± 0.010	0.904 ± 0.014	0.25
Leaf width (µm)	331 ± 10	374 ± 40	315 ± 8	355 ± 13	337 ± 24	0.45

Fully expanded leaves of wild-type *N. tabacum* (WT) and selected lines expressing AtFtsZ1 (FTSZ1-16) AtPDV1 (PDV1-9); AtPDV2 (PDV2-17) and the F1 offspring from lines expressing AtPDV1 and AtPDV2 (PDV2-9 × PDV1-9). Length of diameter at the major (LD; µm) and minor (SD; µm) axis of chloroplasts were measured in three biological replicates with 200 chloroplasts each, with the exception of the large chloroplast line (FTSZ1-16) for which each biological replicate represents between 40 and 52 chloroplasts. The LD and SD were used to calculate chloroplast area, volume, and eccentricity. LD and SD of palisade mesophyll cells, cell number per 100 µm of palisade mesophyll layer, and leaf width were measured in three biological replicates (two technical replicates per biological replicate). From each leaf fragment, six palisade mesophyll cells were measured, the total number of palisade mesophyll cells within the field of view (853.3 × 853.3 µm) was counted, and the leaf width was measured. Length of mesophyll cells exposed to intercellular airspace (L_{mes}), the length of chloroplast exposed to intercellular airspace (L_c); mesophyll surface area exposed to intercellular airspace (S_{mes}) and chloroplast surface area exposed to intercellular airspace (S_c) were measured in four biological replicates with the exception of PDV2-17 ($n = 3$) and each biological replicate represents between two and three fields of view (375.3 × 375.3 µm). All numbers in table represent mean ± SE (n = from 3 to 4 biological replicates). The *P*-values in bold indicate significant effect of the line ($P ≤ 0.05$). Asterisks show a significant difference from WT in Dunnett's two-way test: $P ≤ 0.05$. Data used to produce this figure are given in Datasets S3–S5.

Brown–Forsythe test for homogeneity of variance and the Shapiro–Wilk test for normality. If either test discarded the null hypothesis, data were transformed or a Wilcoxon nonparametric test was performed. One-way analysis of variance (ANOVA) was applied to transcript levels, chloroplast sizes, leaf anatomical and morphological data, chloroplast movement, pigment, absorptance, mesophyll conductance, and gas exchange data. In analysis of biomass dry weight, leaf area, and plant height data from the field experiment, a block was considered as a random effect. Significant line effects in ANOVA ($α = 0.05$) were followed by testing of line means against WT ($α = 0.05$), using Dunnett's multiple comparison correction. Analysis of light absorption profiles was performed using multivariate analysis of variance (MANOVA) and followed by *post hoc* Tukey test ($α = 0.05$).

Results

Molecular phenotype and chloroplast morphology

Relative to WT, the two lines carrying T-DNA of *AtFtsZ1*, FTSZ-11 and -16 had a significant ($P < 0.001$) increase in total (transgenic plus native) *FTSZ1* transcript by 6- and 26-fold, respectively (Fig. 1a; Dataset S1). An additional three lines carrying *AtFTSZ1* T-DNA were also analyzed, but showed lack of transgene expression in T2 homozygous generation (data not shown). From two- to ninefold higher total of *PDVs* expression ($P ≤ 0.002$) was observed for all eight studied lines carrying T-DNA of *SlPDV1* and/or *SlPDV2*. The expression of the transgenes caused a slight reduction in the expression of the corresponding native genes but only in the FTSZ1-11 was the reduction significant ($P = 0.02$) relative to WT.

As expected, disruption of the FtsZ ring via expression of *AtFTSZ1* in tobacco significantly increased chloroplast size (Fig. S4a; Table 1; Dataset S2), as evident from the diameter at the major axis in FTSZ-11 and -16 which was 21% and 218% higher, respectively, than WT ($P ≤ 0.02$; Fig. 1b). The vast size increase of the chloroplasts in FTSZ1 lines led to a significant decrease in the calculated ratio of surface area : volume from −63% to −11% ($P ≤ 0.01$) relative to WT (Fig. 1c). In addition, the deviation from circularity as determined from the eccentricity was larger than WT in FTSZ-16 (16%; $P = 0.003$; Fig. 1d).

Expression of *SlPDV1* and *SlPDV2* in tobacco gave rise to a subtle chloroplast size reduction (Fig. S4; Table 1). For instance, chloroplasts of the F1 hybrid line PDV2-9 × PDV1-9, expressing both *SlPDV1* and *SlPVD2*, significantly differed from WT in six out of seven (Table 1; Dataset S3) analyzed morphological traits of

chloroplasts with a 13% decrease in the major axis diameter ($P=$ 0.005; Fig. 1b). As a result of the decrease in size, the chloroplast surface area : volume ratio was significantly increased (9%, $P=$ 0.02; Fig. 1c) compared with WT. Interestingly, the smaller chloroplasts were more circular than WT, as measured by a significant decrease in eccentricity (-12%; $P=0.02$; Fig. 1d). Based on the chloroplast morphology, line FTSZ1-16 was selected to evaluate the effect of large chloroplasts and lines PDV1-9 and PDV2-17 and PDV2-9 × PDV1-9 were selected to evaluate the effect of small chloroplasts on physiological and growth traits.

Leaf anatomy and morphology

Although chloroplast morphology was significantly different from WT in lines overexpressing FtsZ1, PDV1, and PDV2, this did not seem to give rise to differences in leaf anatomy and morphology (Table 1; Datasets S4, S5). Chloroplast number per cell changed in the opposite direction of chloroplast size differences. Hence, FtsZ1-16 showed a significant reduction in chloroplast number per cell compared with WT ($P=0.0006$) and the small-chloroplast lines had more chloroplasts per cell, although these differences did not pass the significance threshold ($P \geq 0.06$). The ratio between chloroplast surface area adjacent to the intercellular air space and mesophyll surface area exposed to intercellular airspace only marginally differed between lines ($P=0.25$; Table 1).

Chloroplast movements

The ability to undergo chloroplast movements was assessed on the most contrasting chloroplast sizes, that is, lines PDV2-9 × PDV1-9 and FTSZ1-16. Chloroplast movements were estimated from changes in red transmittance during transitions between different chloroplast configurations triggered by blue light with varying intensity. There were no significant differences between the transmittance changes from accumulation to avoidance or avoidance to accumulation configurations of PDV2-9 × PDV1-9, compared with WT (Fig. 2; Dataset S6). However, in line FTSZ1-16, transmittance changed significantly less from accumulation to avoidance position (-60%; $P=0.001$) and from avoidance back to accumulation position (-54%, $P=$ 0.005) compared with WT (Fig. 2a,b). A significant genotype effect ($P=0.02$) was found for the time constant of the transition from accumulation to avoidance configuration, mainly driven by the faster transitions observed in FTSZ1-16 (Fig. 2c). The time constants for the transition from avoidance to accumulation configuration were similar in all three lines.

Leaf absorptance and pigment composition

Spectrometric analysis of pigment extract showed significant decreases in the chl$a$: chl$b$ ratio (-9%; $P=0.04$) and carotenoids (-15%; $P=0.005$) in line FTSZ1-16 relative to WT (Table 2; Dataset S7). The small-chloroplast lines did not show any significant differences compared with WT. Despite the differences in pigment composition in FTSZ1-16, absorptance of leaves from all lines was relatively similar, with only small, but
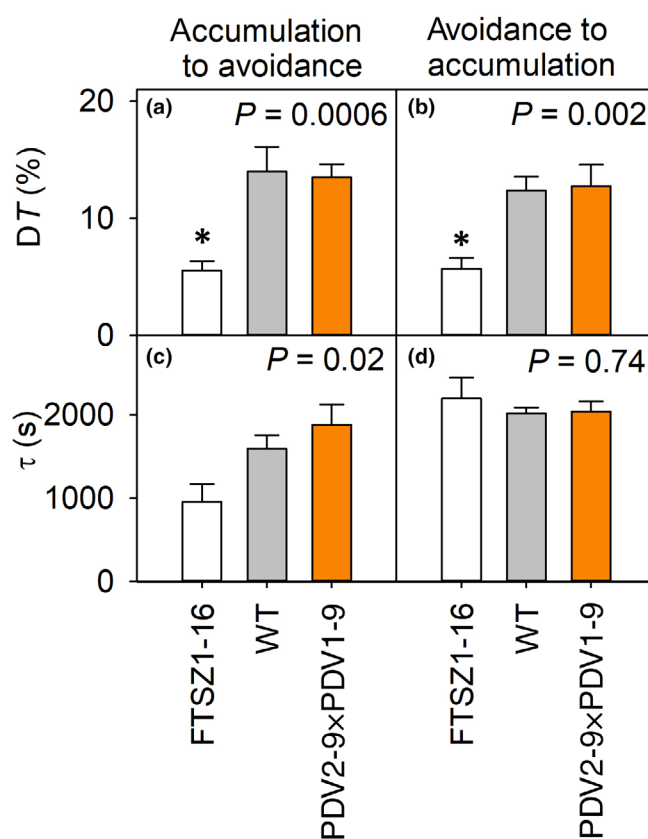

Fig. 2 Chloroplast movement in *Nicotiana tabacum* with modified chloroplast sizes and corresponding wild-type. (a, b) Percentage of light transmittance relative to the value measured before turning on the blue light and (c, d) time constant for the youngest fully expanded leaves of wild-type (WT) and lines with large (FTSZ1-16) and smaller (PDV2-9 × PDV1-9) chloroplasts. (a, c) show the characteristics of chloroplast movement from accumulation to avoidance position (from low to high light); (b, d) show the characteristics of chloroplast movement from avoidance to accumulation position (from high back to low light). Plants were grown in the growth chamber. Error bars indicate SE ($n=$ from 6 to 7 biological replicates). The P-values indicate the effect of the line. Asterisks show a significant difference from WT in Dunnett's two-way test: $P \leq 0.05$. Data used to produce this figure are given in Dataset S6.

significant decreases of *c.* 3–4% ($P \leq 0.04$) in the green spectral region for FTSZ1-16, PDV1-9 and PDV2-17 compared with WT and even smaller decreases (-1%, $P \leq 0.03$) in the red region for FTSZ1-16 and PDV2-17 (Table 2; Dataset S8).

Leaf internal light profiles

Although measurements of leaf absorptance were relatively similar across the lines with both larger and smaller chloroplasts, this does not necessarily imply that light absorption profiles within the leaf were similarly unaltered. To find out whether light attenuation profiles across the leaf vertical axis were impacted by the different chloroplast sizes and shapes, light-sheet microscopy was performed on leaves at four different wavelengths covering the spectral range of photosynthetically active radiation. Table 3 shows the percentage of total absorbed light at different leaf depths (Dataset S9). Absorption of light at 561 nm across the

Table 2 Quantification of photosynthesis-related pigments and absorptance of irradiance in glasshouse-grown lines *Nicotiana tabacum* with contrasting chloroplast sizes.

Parameter	FTSZ1-16	WT	PDV1-9	PDV2-17	PDV2-9 × PVD1-9	*P*-value
Pigments (mg m^{-2})						
Chla	420 ± 19	480 ± 12	463 ± 21	455 ± 5	474 ± 9	0.06
Chlb	120 ± 7	125 ± 6	129 ± 7	125 ± 4	123 ± 4	0.86
Chlab	540 ± 26	605 ± 17	592 ± 28	580 ± 3	597 ± 12	0.18
Chla/b	3.51 ± 0.08*	3.87 ± 0.10	3.60 ± 0.06	3.66 ± 0.17	3.86 ± 0.07	**0.05**
Car	108 ± 4*	127 ± 3	121 ± 4	120 ± 4	121 ± 2	**0.02**
Car/Chlab	0.201 ± 0.004	0.210 ± 0.004	0.208 ± 0.014	0.206 ± 0.006	0.203 ± 0.005	0.92
Car/Chlb	0.906 ± 0.026	1.023 ± 0.036	0.959 ± 0.074	0.965 ± 0.061	0.984 ± 0.031	0.54
Absorptance						
Blue	0.926 ± 0.002	0.929 ± 0.001	0.926 ± 0.001	0.925 ± 0.001	0.927 ± 0.001	0.15
Green	0.693 ± 0.004*	0.719 ± 0.006	0.697 ± 0.005*	0.692 ± 0.006*	0.713 ± 0.006	**0.004**
Red	0.873 ± 0.002*	0.884 ± 0.003	0.875 ± 0.003	0.871 ± 0.003*	0.884 ± 0.002	**0.005**

The fully expanded leaves of lines with big (FTSZ1-16) and small chloroplasts (PDV1-9, PDV2-17 and PDV2-9 × PDV1-9) and wild-type *N. tabacum* (WT) were used in analyses. The chlorophyll a (*Chla*), chlorophyll b (*Chlb*) and carotenoids (*Car*) contents were estimated on the leaf extract with the use of spectrometer. Average absorptance was measured for the full spectrum of photosynthetically active irradiance (i.e. between 400 and 700 nm). Average values were calculated for a range of wavelengths: 450–490 nm (blue) 540–560 nm (green) and 610–660 nm (red). Means ± SE are shown (n = from 5 to 6 biological replicates for pigment analyses and n = 6 biological replicates for absorbance analyses). The *P*-values in bold indicate the significant effect of the line (*P* ≤ 0.05). Asterisks show a significant difference from WT in Dunnett's two-way test: *P* ≤ 0.05. Data used to produce this figure are given in Datasets S7, S8.

three depth intervals was relatively similar for all lines in the non-infiltrated samples. For the more strongly absorbed wavelengths 405 and 488 nm, absorption of light in PDV1-9 and PDV2-9 × PDV1-9 leaves showed a significant shift from the upper (0–100 µm) to midleaf (100–200 µm) relative to WT (*P* < 0.05), and measurements at 638 nm showed a similar trend. In the infiltrated samples, where internal scattering is reduced by phase changes and thereby a shorted effective path length, relative absorption in all transgenic lines tended to show a similar shift from 0–100 to 100–200 µm, relative to WT. This trend was significant for measurements at 405 and 488 nm in the lines with the most contrasting chloroplast sizes (FTSZ1-16 and PDV2-9 × PDV1-9). Thus, light absorption occurred generally deeper in leaves with smaller chloroplasts, while remaining relatively similar in leaves with larger chloroplasts. The comparison with the infiltrated samples may imply that internal scattering increases superficial absorptance, most significantly in leaves with larger chloroplasts.

Effect of chloroplast size on photosynthetic electron transport and CO$_2$ assimilation

To determine the effect of contrasting chloroplast sizes on photosynthetic efficiency, light-response curves (90% red and 10% blue light) of net CO$_2$ assimilation (A_n) and photosynthetic electron transport (J) were measured in parallel. A_n was markedly decreased in leaves with larger chloroplasts (FTSZ1-16; Fig. 3a; Dataset S10), especially at higher light intensities. At 2000 µmol m^{-2} s^{-1}, average A_n in FTSZ1-16 was 30% lower than in WT leaves (*P* = 0.003; Fig. 3b). By contrast, the lines with smaller chloroplasts were not significantly affected compared with WT, although PDV2-17 trended lower than WT, especially at higher light intensities. Consistent with the A_n measurements, J was significantly perturbed by the enhanced chloroplast size in FTSZ1-16 (Fig. 3b), which could be seen most prominently (*P* = 0.002)

in the asymptote value which was 43% lower than in WT (J_{max}; Fig. 3c). In addition, slightly lower values for J were measured in PDV2-17, relative to WT. However, this difference seemed unrelated to the reduced chloroplast size in PDV2-17, since J in PDV2-9 × PDV1-9 with the smallest chloroplast size was unaffected. Consistent with the reduction in photochemical quenching in FTSZ1-16, NPQ levels were significantly higher than WT (Fig. 3g). This was reflected both in the NPQ level at 2000 µmol m^{-2} s^{-1}, which was significantly higher (*P* = 0.002; Fig. 3e) as well as in a significantly lower value of K_{NPQ} (*P* = 0.004; Fig. 3f) which signifies the light intensity at which NPQ has reached half-maximum levels (499 vs 1089 µmol m^{-2} s^{-1}, for FTSZ1-16 and WT, respectively).

The light-response measurements were repeated using 100% red light to find out whether any of the responses in Fig. 3 were affected by the differential ability of the lines to undergo chloroplast movements (Fig. 2). However, results were very similar (Fig. S5; Table S2; Dataset S11). The lines were also subjected to a fluctuating light regime from which light-response curves could be reconstructed, but again, significant differences were only detected between the FTSZ1-16 and WT (Fig. S6; Table S2; Dataset S12). In fact, almost identical differences in J_{max} (−44%; *P* < 0.0001) and A_{sat} (−31%, *P* = 0.0001) were observed between FTSZ1-16 compared with WT in both steady-state and dynamic light-response curves.

To assess whether the differences in A_n and J could be explained by differences in biochemical capacity, CO$_2$ response curves were performed (Fig. 4a; Dataset S13). A_n in FTSZ1-16 increased less steeply with increasing C_i and also reached a lower plateau at saturating CO$_2$. Discrimination against ^{13}CO$_2$ was used to determine whether the decreased slope could result from a decline in the conductance to CO$_2$ from the intercellular airspaces to the point of fixation (g_m). Indeed, g_m was significantly lower in FTSZ1-16 compared with WT under low O$_2$ as well as ambient O$_2$ levels (Fig. 4b; Dataset S14). The hypothesized

Table 3 Profiles of light absorption in leaves of growth-chamber-grown *Nicotiana tabacum* with contrasting chloroplast sizes.

Depth (µm)	Line	Non-infiltrated				Infiltrated			
		405 nm	488 nm	561 nm	638 nm	405 nm	488 nm	561 nm	638 nm
0–100	FTSZ1-16	36 ± 3% c	33 ± 1% ab	26 ± 2% a	32 ± 4% ab	25 ± 2% b	18 ± 2% a	13 ± 1% ab	19 ± 2% a
	WT	34 ± 5% bc	39 ± 7% b	24 ± 4% a	32 ± 6% ab	43 ± 4% c	42 ± 6% b	27 ± 5% b	25 ± 2% ab
	PDV1-9	20 ± 2% a	21 ± 1% a	21 ± 4% a	25 ± 1% a	40 ± 3% c	33 ± 3% b	17 ± 3% ab	27 ± 3% ab
	PDV2-17	41 ± 3% c	43 ± 1% b	31 ± 2% a	37 ± 1% b	46 ± 6% c	40 ± 8% b	25 ± 4% b	36 ± 4% b
	PDV2-9 × PDV1-9	23 ± 4% a	24 ± 3% a	20 ± 4% a	27 ± 2% ab	11 ± 4% a	21 ± 7% a	10 ± 3% a	25 ± 6% ab
100–200	FTSZ1-16	42 ± 1% ab	46 ± 3% ab	45 ± 2% a	44 ± 1% a	47 ± 2% b	52 ± 2% bc	44 ± 2% a	46 ± 3% a
	WT	41 ± 1% ab	41 ± 2% ab	46 ± 3% a	45 ± 1% a	34 ± 1% a	36 ± 0% a	38 ± 1% a	41 ± 2% a
	PDV1-9	52 ± 2% b	53 ± 3% b	47 ± 2% a	50 ± 2% a	42 ± 4% ab	51 ± 3% bc	48 ± 1% ab	48 ± 2% a
	PDV2-17	36 ± 2% a	40 ± 1% a	42 ± 2% a	41 ± 1% a	34 ± 3% ab	41 ± 2% ab	42 ± 2% ab	42 ± 2% a
	PDV2-9 × PDV1-9	51 ± 5% b	52 ± 6% ab	46 ± 3% a	48 ± 4% a	62 ± 3% c	55 ± 2% c	50 ± 2% b	47 ± 1% a
200–300	FTSZ1-16	14 ± 2% a	16 ± 2% a	19 ± 3% a	18 ± 4% a	20 ± 0% a	24 ± 1% a	30 ± 1% a	27 ± 1% a
	WT	17 ± 5% a	16 ± 5% a	22 ± 5% a	18 ± 5% a	15 ± 3% a	16 ± 3% a	23 ± 3% a	25 ± 3% a
	PDV1-9	20 ± 5% a	21 ± 5% a	24 ± 5% a	20 ± 2% a	11 ± 0% a	13 ± 1% a	24 ± 3% a	20 ± 2% a
	PDV2-17	14 ± 2% a	12 ± 1% a	18 ± 1% a	15 ± 1% a	12 ± 3% a	15 ± 4% a	22 ± 3% a	16 ± 3% a
	PDV2-9 × PDV1-9	18 ± 1% a	18 ± 3% a	23 ± 5% a	19 ± 4% a	20 ± 2% a	19 ± 4% a	28 ± 3% a	22 ± 4% a

Effect	*P*-value
Line (L)	0.98
Wavelength (WL)	0.16
Leaf depth (D)	**< 0.0001**
Infiltration (I)	0.59
L × D	**< 0.0001**
L × WL	1.00
L × I	0.96
D × I	**0.009**
WL × D	**< 0.0001**
WL × I	0.90
L × D × I	**< 0.0001**
L × WL × I	1.00
L × WL × D	**0.001**
WL × D × I	**0.04**
L × WL × D × I	0.14

The fully expanded leaves of lines with big (FTSZ1-16) and small chloroplasts (PDV1-9, PDV2-17 and PDV2-9 × PDV1-9) and wild-type *N. tabacum* (WT) were used in analyses. Light profiles were measured using light-sheet microscopy at four different excitation wavelengths on leaf samples with and without prior water infiltration. Light absorption was determined from chlorophyll fluorescence (detected between 705 and 800 nm) as a function of leaf depth. Results are shown as the percentage absorbed light at each depth (average ± SE, $n = 3$ biological replicates for infiltrated and non-infiltrated leaves). In MANOVA table significant effects and interactions are shown by bold font ($P \leq 0.05$). Genotypes with different letters within each treatment combination of excitation wavelength, infiltration treatment, and depth are significantly different ($P \leq 0.05$) based on *post hoc* Tukey testing. Data used to produce this figure are given in Dataset S9.

increase in g_m because of increased surface : volume ratio in the smaller chloroplast size line, PDV2-9 × PDV1-9, was not observed, and instead, g_m was indistinguishable from WT. Biochemical capacities were derived from data in Fig. 4a yielding significant decreases in V_{cmax}, J and TPU in FTSZ1-16, relative to WT. No significant impact of smaller chloroplast size on V_{cmax}, J or TPU could be observed (Fig. 4c–e; Table S3).

Performance under field conditions

Finally, to determine whether chloroplast size impacted performance under field conditions, FTSZ1-16, PDV2-17, PDV2-9 × PDV1-9, and WT plants were grown in a randomized complete block design of 12 blocks (Fig. S2). The previously observed chloroplast size and shape differences were confirmed (Fig. S7; Dataset S15), with the exception of eccentricity which in field

conditions was only significantly different from WT in FTSZ1-16. Pigment analysis showed a lack of significant differences between lines (Table S4; Dataset S16). Nevertheless, absorbance in the green (−5%; $P = 0.02$) and the red (−3%; $P = 0.005$) spectral regions were significantly decreased in FTSZ1-16 (Table S4; Dataset S17).

Light-response curves of J and A_n in FTSZ-16 showed a 38% ($P = 0.02$) decrease in J_{max} and 22% ($P = 0.007$) decrease in A_{sat} in relation to WT (Fig. S8; Table S2; Dataset S18). Similar to the measurements under controlled conditions, C_i throughout the light-response curves was higher in FTSZ-16 than WT, whereas stomatal conductance was similar across all lines. The A_n/C_i response of FTSZ-16 showed a slight decrease in initial slope and asymptote (Fig. S9; Dataset S19). However, differences were less pronounced than under controlled conditions and biochemical parameters fitted on these measurements did not differ
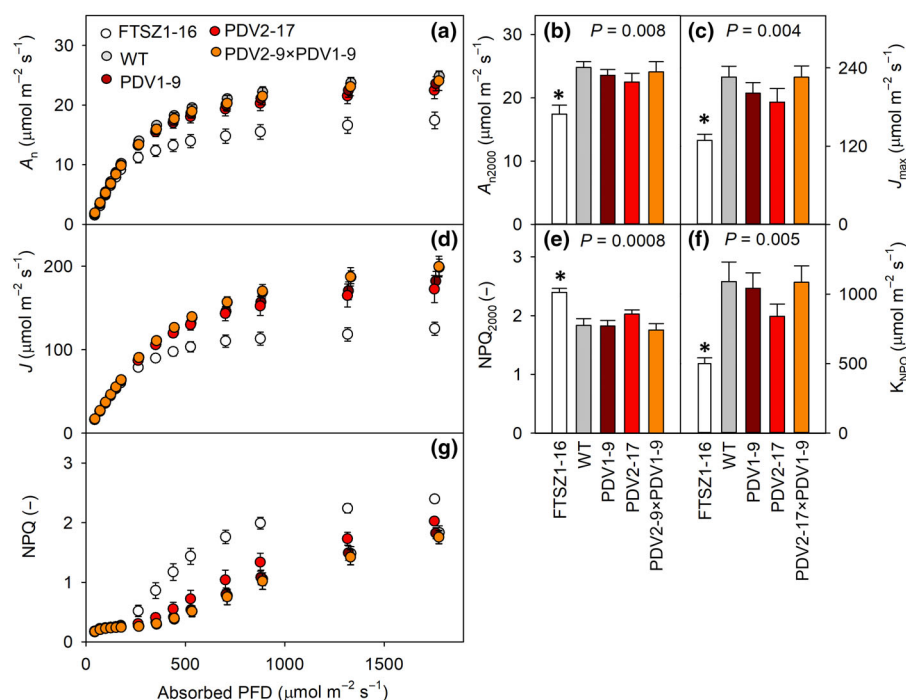
Fig. 3 Response of gas exchange and fluorescence parameters to steady-state light (90% red and 10% blue) in glasshouse-grown *Nicotiana tabacum* with modified chloroplast sizes. Light levels were increased from low to high incident photon flux density (PFD), while waiting for steady state at each step. (a) Net CO_2 fixation rate (A_n), (d) linear electron transport (J) and (g) non-photochemical quenching (NPQ) as a function of absorbed PFD. (b) A_n and (e) NPQ at the light intensity of 2000 µmol m^{-2} s^{-1}. (c) The maximum rate of linear electron transport (J_{max}). (f) The PFD in which NPQ reaches half of its maximum value (K_{NPQ}). Measurements were for the youngest fully expanded leaves of wild-type (WT) and lines with larger (FTSZ1-16) and smaller (PDV1-9, PDV2-17, and PDV2-9 × PDV1-9) chloroplasts. Error bars indicate SEM (n = from 5 to 6 biological replicates). In panels (b, c, e, f) the P-values indicate the effect of the line and asterisks show a significant difference from WT in Dunnett's two-way test: $P \leq 0.05$. Data used to produce this figure are given in Dataset S10.

significantly (Table S4). Pigment content, absorptance, and gas exchange parameters of field-grown PDV2-17 and PDV1-9 × PDV2-9 were indistinguishable from WT (Tables S2–S4).

Although no significant genotypic differences were found for size and productivity parameters, the lines with largest (FTSZ1-16) and smallest (PDV2-9 × PDV1-9) chloroplasts both trended negatively compared with WT (Figs 5, S10; Dataset S20). The FTSZ1-16 showed lower total dry weight (−10%; $P = 0.4$), leaf area (−8%; $P = 0.4$), and plant height (−1%; $P = 0.9$), while the plants of PDV2-9 × PDV1-9 showed decreases in total dry weight (−11%; $P = 0.3$), leaf area (−13%; $P = 0.1$), and plant height (−5%; $P = 0.2$). The line with only minor decrease in chloroplast size (PDV2-17) was very similar in size and weight compared with WT (Fig. 5).

Discussion

Increasing chloroplast size decreases g_m but decreasing chloroplast size does not increase g_m

Expressing *AtFtsZ1* in tobacco resulted in a threefold increase in chloroplast diameter at the major axis compared with WT. As a consequence, the ratio of chloroplast surface area : volume declined (−63%) whereas the eccentricity increased (+15%; Fig. 1; Table 1). The biochemical capacities V_{cmax}, J_{max}, and TPU were lower in the FTSZ1-16 than in WT (Figs 4, S9; Table S3), but this does not appear a universal phenotype of large-chloroplast mutants. For example, *A. thaliana* arc3 mutants with c. 14 chloroplasts per cell (similar to FTSZ1-16 reported here) resulted in an opposite phenotype where V_{cmax}, J_{max}, and TPU were higher than in WT (Weise *et al.*, 2015). The changes in size and shape of chloroplasts in FTSZ1-16 were associated

with a significant decrease in g_m (Fig. 4b). Depending on the oxygen concentration (ambient or reduced), g_m was reduced from −46% to −22% relative to WT. The more pronounced reduction under photorespiratory conditions is consistent with the apparent effect of photorespiration on g_m when the chloroplast envelope imposes a significant resistance to CO_2 transfer as outlined by Tholen and Zhu (2011). A decrease in g_m of similar magnitude was seen in *arc* mutants of *A. thaliana*, which also have significantly enlarged chloroplasts (Weise *et al.*, 2015; Xiong *et al.*, 2017). The chloroplast surface exposed to intercellular airspaces, S_c/S_{mes}, was not significantly affected by the size increase, hence did not underlay the decrease in g_m in FTSZ1-16 (Table 1). Instead, it is possible that the increase in stromal volume per unit chloroplast envelope may have presented additional resistance to CO_2 transfer.

The ectopic expression of *SlPDV1* and *SlPDV2* and especially their combination in the cross between PDV2-9 and PDV1-9, caused a reduction of chloroplast diameter at the major axis by up to 12% (Fig. 1; Table 1). The synergistic effect of PDV1 and PDV2 is in line with the overexpression of *AtPDV1* and *AtPDV2* in *A. thaliana*, which also yielded significantly smaller and more abundant chloroplasts per cell than overexpression of PDVs separately (Okazaki *et al.*, 2009). The decreases in chloroplast diameter at the major axis were also manifested in both increases in the estimated ratio of chloroplast surface area : volume (+9%) and decreases in eccentricity (−12%). Although the increase in surface : volume ratio was hypothesized to alleviate the impact of chloroplast envelope resistance on g_m (Tholen & Zhu, 2011), g_m was instead found to be similar to WT. It is not entirely clear why g_m did not increase in the smaller chloroplast lines. One possible explanation is that the concomitant change in eccentricity may have negated any positive impact due to the increase in

Fig. 4 Inferred biochemical capacity of photosynthesis in *Nicotiana tabacum* with modified chloroplast sizes under glasshouse conditions. (a) Net CO_2 fixation rate (A_n) as a function of intercellular CO_2 concentration (C_i), (b) mesophyll conductance estimated from carbon isotope discrimination ($\Delta^{13}C$) measured in conjunction with photosynthetic gas exchange under 2 and 21% of oxygen concentration, (c) maximum ribulose bisphosphate carboxylation capacity (V_{cmax}), (d) rate of linear electron transport (J) and (e) rate of triose phosphate utilization (TPU). Measurements were for the youngest fully expanded leaves of WT, and of lines with larger (FTSZ1-16) and smaller (PDV1-9, PDV2-17, and PDV2-9 × PDV1-9) chloroplast sizes than WT. Error bars indicate SE (biological replicates were $n =$ from 5 to 6 plants in panels (a, c–e) and, $n =$ from 3 to 4 in panel (b)). In panels (b–e) the P-values indicate the effect of the line and asterisks show a significant difference from WT in Dunnett's two-way test: $P \leq 0.05$. Data used to produce this figure are given in Datasets S13, S14.
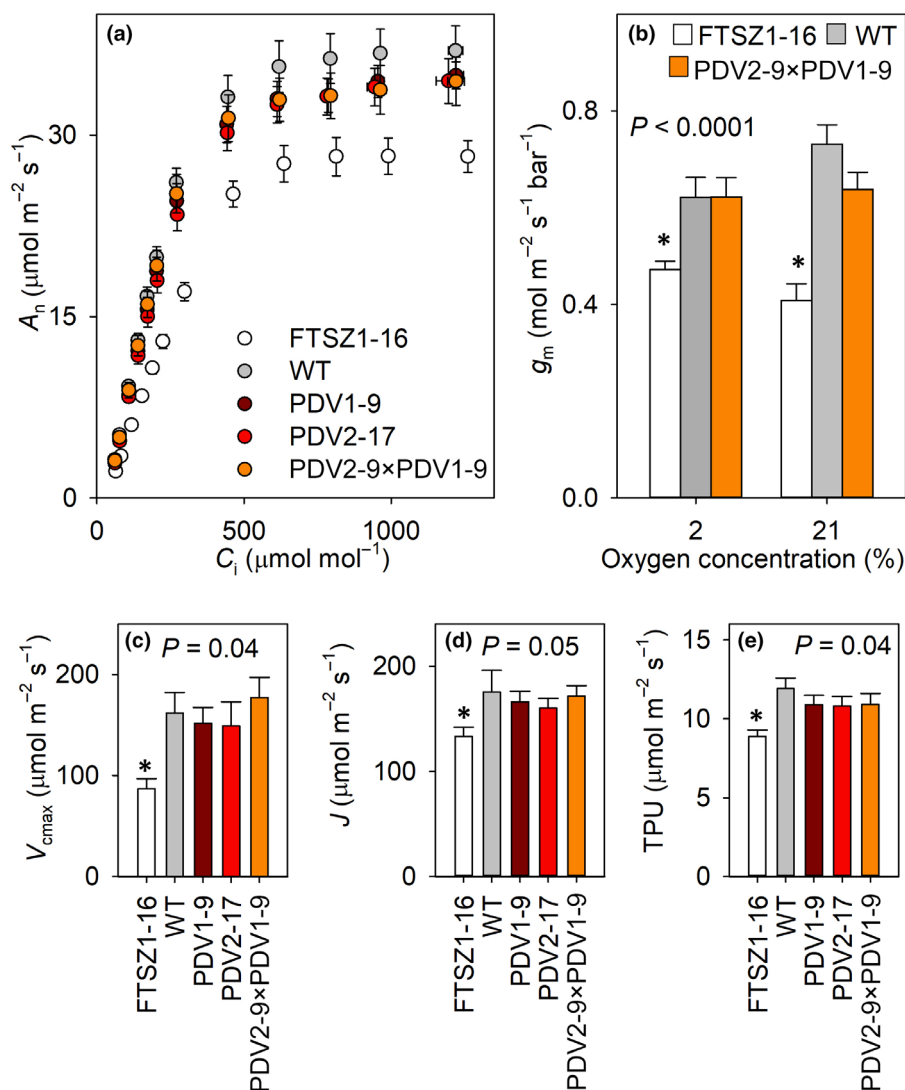
surface : volume ratio. Evans (2021) noted a relationship between g_m and the surface area of the plastids adjacent to air spaces. While we might expect this to be increased with smaller chloroplasts, these were more spherical than the larger WT chloroplasts, which could have reduced direct contact with the plasmalemma and wall adjacent to the air space.

Chloroplast size only weakly affects light absorptance and light profiles within the leaf

Due to the hyperbolic response of net CO_2 assimilation to light intensity, light absorptance profiles which closely match the distribution in photosynthetic capacity are theoretically most favorable for photosynthetic efficiency (Evans & Vogelmann, 2003). Light absorptance within the leaf is a function of the concentration and distribution of absorbing pigments, in particular chlorophylls. In addition, internal scattering can strongly increase the effective light path length and thereby affect light profiles (Vogelmann & Evans, 2002). Whole-leaf absorptance was relatively similar between all lines, despite significant

decreases in chl$a$: chl$b$ ratio and carotenoid concentration in the FTSZ1-16 (Table 2). Light absorption profiles were also relatively unperturbed in the FTSZ1-16, where the decline in pigment concentration appeared to be compensated by the path-lengthening effect of leaf internal scattering (Table 3). In the lines with smaller chloroplasts, light penetrated more deeply into the leaf, but this did not seem to affect the light response of photochemistry or CO_2 assimilation, suggesting that the change was not sufficient enough to impact photosynthetic efficiency. This is consistent with photosynthesis in low-chlorophyll soybean mutants, where leaf-level photosynthesis was only affected when chlorophyll content was decreased by $> 50\%$ (Slattery *et al.*, 2016).

Increasing chloroplast size reduces chloroplast movements and increases non-photochemical dissipation of excitation energy

The increase in chloroplast size in FTSZ1-16 impaired both the ability to undergo chloroplast movement in response to light
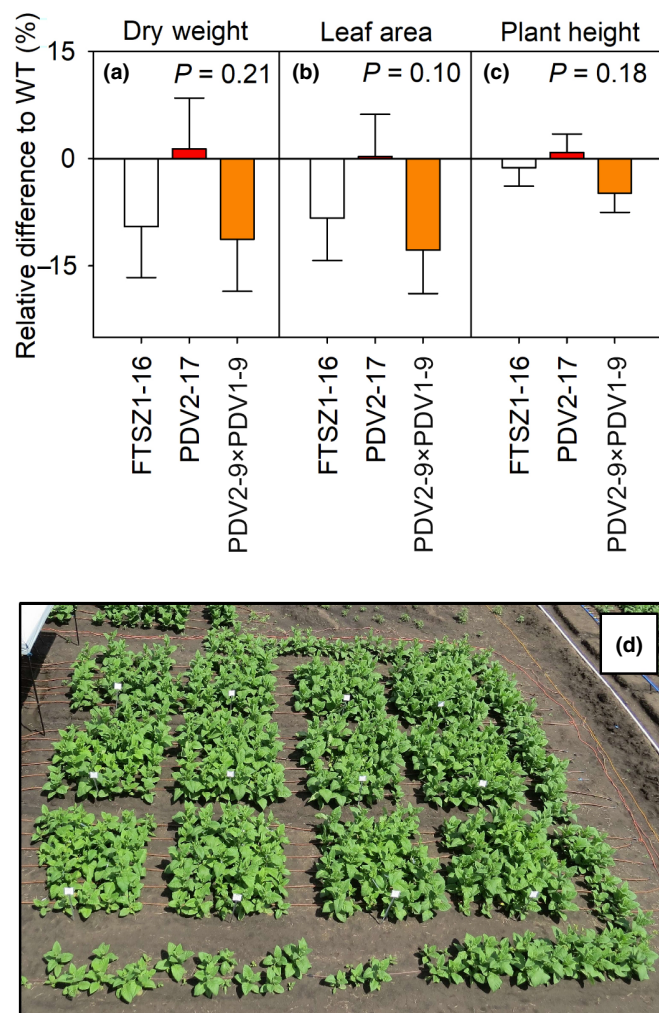
Fig. 5 Productivity of field-grown *Nicotiana tabacum* plants with modified chloroplast sizes. (a) Total dry weight, (b) leaf area, and (c) plant height for the large-chloroplast line (FTSZ1-16) and small-chloroplast lines (PDV2-17 and PDV2-9 × PDV1-9). (d) Aerial view of the field experiment. Data were normalized to wild-type (WT). Error bars indicate SE (*n* = 12 blocks with the exception of PDV2-9 × PDV1-9 for which 11 blocks were analyzed). The *P*-values indicate the effect of the line. No significant differences between WT and lines with modified chloroplast sizes were found in Dunnett's two-way test: *P* ≤ 0.05. Data used to produce this figure are given in Dataset S20.

increase and decrease (Fig. 2). A similar effect of enlarged chloroplasts on photorelocation was shown for chloroplast division mutants of *A. thaliana* (Austin & Webber, 2005; Königer et al., 2008; Dutta et al., 2017) and FTSZ1-overexpressing tobacco (Jeong et al., 2002). Chloroplast movement depends on short actin filaments (cp-actin) specific to chloroplast movement (Wada & Kong, 2019). Increasing plastid size may reduce the ability of cp-actin to move the organelle relative to WT. Mutants with enlarged chloroplasts have been reported to be more sensitive to fluctuating light (Dutta et al., 2015). However, we did not see a stronger phenotype for FTSZ1-16 when comparing steady state with the dynamic response of NPQ, A_n, and J to varying light intensities (Figs 3, S6; Table S2). The impairment of chloroplast movement can make plants to be more prone to

photoinhibition (e.g. Wada et al., 2003). Previous studies on *A. thaliana* and tobacco with enlarged chloroplasts (Jeong et al., 2002; Dutta et al., 2015) also reported photobleaching and unusually strong midday depression of ΦPSII but neither of these were observed in the FTSZ1-16 when grown in the glasshouse or field. NPQ levels did increase at much lower light levels in the FTSZ1-16 compared with the WT or lines with reduced chloroplast size (Fig. 3; Table S2). However, this did not seem to be caused by the reduced ability to undergo chloroplast movements, since the same observations were also found in the absence of blue light (Fig. S5).

Whereas the drawbacks of larger chloroplast size were obvious for chloroplast movements and NPQ, the reduction in chloroplast size seemed to have very little impact on any of these parameters. Levels of NPQ under steady-state and fluctuating light were very similar to WT and the ability to undergo chloroplast movements also seemed unperturbed in both the magnitude and rate of change (Fig. 2). As far as we are aware, this is the first time that these parameters have been determined on lines with smaller chloroplasts. Altogether, the results suggest that the ability to undergo chloroplast movements or avoid photosensitivity is likely to be determinants of the upper, but not the lower limit of chloroplast size (Figs 2, 3).

Changing chloroplast size did not significantly affect productivity under field conditions

Despite findings of a number of photosynthetic inefficiencies in the large-chloroplast line, there was little effect on biomass production when plants were grown in well-watered and well-fertilized field conditions. The weak decrease in productivity in the FTSZ1-16, albeit nonsignificant, was consistent with the photosynthetic phenotype, which was confirmed for the field-grown plants (Figs 5, S8–S10). This decline in productivity could have resulted directly from the lower net CO_2 assimilation. It may also be negatively affected by the decline in intrinsic water use efficiency (Table S2). In addition, the stressful outdoor conditions in the middle of the day can still create temporary mild drought stress, even though soil water levels were restored to field capacity each evening. As a result, the lower intrinsic water use efficiency found in the FTSZ1-16 could have been an alternative explanation for the decline in productivity. When the native FTSZ1 gene was overexpressed in tobacco under the strong constitutive promoter, Jeong et al. (2002) observed in high-light conditions a far more severe reduction in growth compared with WT. In their study, fresh plant weight, leaf area of the youngest fully expanded leaf, and plant height of the mutant line were reduced by 32%, 32%, and 47%, respectively. These differences probably result from the stronger reduction of chloroplast number (one to two big chloroplasts per cell) in the line used by Jeong et al. (2002) in comparison with the FTSZ1-16 used in our study (on average 14 chloroplasts per cell).

The plants with the most severe reduction in chloroplast size (PDV2-9 × PDV1-9) also showed a weak decline in productivity, whereas the minor decrease in chloroplast size in PDV2-17 did not impact plant size or dry weight (Figs 5, S10). This is the first

time that small-chloroplast mutants have been evaluated under field conditions. The results suggest that there is a lower limit for chloroplast size, below which plants grow less efficiently. However, we did not find any evidence in the photosynthetic efficiency phenotypes to derive the mechanistic reasons for the productivity decline, since the small-chloroplast lines behaved very similar to WT plants in every trait evaluated. However, we can speculate that beyond a lower size limit, the economy of producing ever smaller chloroplasts will disrupt the balance between membrane and soluble fractions and associated synthesis costs. It may be that these are the main determinants for the lower limit of chloroplast size. Based on the findings presented here, we conclude that manipulations of chloroplast size are unlikely to achieve higher photosynthetic efficiency or growth.

Competing interests

None declared.

Author contributions

KG and JK designed the experiments, in consultation with SPL. KG selected and verified homozygous transgenic lines and F1 hybrid, performed Nomarski optics and light-sheet microscopy, and measured chloroplast movement, pigments, gas exchange, and fluorescence. CS performed chloroplast size measurements. KG and CS performed the transcript quantification. CES-S performed leaf anatomical analyses. JK performed carbon isotope discrimination analysis and extracted data from chloroplast movement and light-sheet microscopy data. KG, JK, and SMD performed field experiment. KG and SMD collected physiological measurements from field. KG performed statistical analyses. KG and JK wrote the manuscript with contributions from all the authors. All authors reviewed and approved of the manuscript.

ORCID

Steven M. Driever https://orcid.org/0000-0003-4144-6028
Katarzyna Głowacka https://orcid.org/0000-0002-8892-1482
Johannes Kromdijk https://orcid.org/0000-0003-4423-4100
Stephen P. Long https://orcid.org/0000-0002-8501-7164
Coralie E. Salesse-Smith https://orcid.org/0000-0002-2856-4217
Cailin Smith https://orcid.org/0000-0002-0188-806X

Data availability

The data that support the findings of this study are available in the supplementary material of this article.

References

Alexandratos N, Bruinsma J. 2012. *World agriculture towards 2030/2050: the 2012 revision.* ESA Working Paper No. 12-03. Rome, Italy: FAO.

Austin J, Webber AN. 2005. Photosynthesis in *Arabidopsis thaliana* mutants with reduced chloroplast number. *Photosynthesis Research* **85**: 373–384.

Bailey-Serres J, Parker JE, Ainsworth EA, Oldroyd GED, Schroeder JI. 2019. Genetic strategies for improving crop yields. *Nature* **575**: 109–118.

Banaś AK, Aggarwal C, Łabuz J, Sztatelman O, Gabryś H. 2012. Blue light signalling in chloroplast movements. *Journal of Experimental Botany* **63**: 1559–1574.

Bilger W, Björkman O. 1994. Relationships among violaxanthin deepoxidation, thylakoid membrane conformation, and nonphotochemical chlorophyll fluorescence quenching in leaves of cotton (*Gossypium hirsutum* L.). *Planta* **193**: 238–246.

Clemente T. 2006. Nicotiana (*Nicotiana tobaccum, Nicotiana benthamiana*). In: Wang K, ed. *Agrobacterium protocols.* Totowa, NJ, USA: Humana Press, 143–154.

Dalin C, Wada Y, Kastner T, Puma MJ. 2017. Groundwater depletion embedded in international food trade. *Nature* **543**: 700–704.

De Souza AP, Burgess SJ, Doran L, Hansen J, Manukyan L, Maryn N, Gotarkar D, Leonelli L, Niyogi KK, Long SP. 2022. Soybean photosynthesis and crop yield are improved by accelerating recovery from photoprotection. *Science* **377**: 851–854.

Dutta S, Cruz JA, Imran SM, Chen J, Kramer DM, Osteryoung KW. 2017. Variations in chloroplast movement and chlorophyll fluorescence among chloroplast division mutants under light stress. *Journal of Experimental Botany* **68**: 3541–3555.

Dutta S, Cruz JA, Jiao Y, Chen J, Kramer DM, Osteryoung KW. 2015. Non-invasive, whole-plant imaging of chloroplast movement and chlorophyll fluorescence reveals photosynthetic phenotypes independent of chloroplast photorelocation defects in chloroplast division mutants. *The Plant Journal* **84**: 428–442.

Engler C, Gruetzner R, Kandzia R, Marillonnet S. 2009. Golden gate shuffling: a one-pot DNA shuffling method based on type IIs restriction enzymes. *PLoS ONE* **4**: e5553.

Ermakova M, Lopez-Calcagno PE, Raines CA, Furbank RT, von Caemmerer S. 2019. Overexpression of the Rieske FeS protein of the cytochrome b_6f complex increases C_4 photosynthesis in *Setaria viridis*. *Communications Biology* **2**: 1–12.

Evans J, von Caemmerer S, Setchell BA, Hudson GS. 1994. The relationship between CO_2 transfer conductance and leaf anatomy in transgenic tobacco with a reduced content of Rubisco. *Australian Journal of Plant Physiology* **21**: 475–495.

Evans JR. 2021. Mesophyll conductance: walls, membranes and spatial complexity. *New Phytologist* **229**: 1864–1876.

Evans JR, Sharkey TD, Berry JA, Farquhar GD. 1986. Carbon isotope discrimination measured concurrently with gas exchange to investigate CO_2

diffusion in leaves of higher plants. *Australian Journal Plant Physiology* **13**: 281–292.

Evans JR, Vogelmann TC. 2003. Profiles of ^{14}C fixation through spinach leaves in relation to light absorption and photosynthetic capacity. *Plant, Cell & Environment* **26**: 547–560.

Evans JR, Von Caemmerer S. 2013. Temperature response of carbon isotope discrimination and mesophyll conductance in tobacco. *Plant, Cell & Environment* **36**: 745–756.

FAO, IFAD, UNICEF, WFPW. 2020. *Food security and nutrition in the world.*

Farquhar GD, Von Caemmerer S, Berry J. 1980. A biochemical model of photosynthesis CO_2 fixation in leaves of C_3 species. *Planta* **149**: 78–90.

Genty B, Briantais J-M, Baker NR. 1989. The relationship between quantum yield of photosynthetic electron transport and quenching of chlorophyll fluorescence. *Biochimica et Biophysica Acta* **990**: 89–92.

Głowacka K, Kromdijk J, Leonelli L, Niyogi KK, Clemente TE, Long SP. 2016. An evaluation of new and established methods to determine T-DNA copy number and homozygosity in transgenic plants. *Plant, Cell & Environment* **39**: 908–917.

Hunter MC, Smith RG, Schipanski ME, Atwood LW, Mortensen DA. 2017. Agriculture in 2050: recalibrating targets for sustainable intensification. *Bioscience* **67**: 386–391.

Jeong WJ, Park YI, Suh KH, Raven JA, Ook JY, Jang RL. 2002. A large population of small chloroplasts in tobacco leaf cells allows more effective chloroplast movement than a few enlarged chloroplasts. *Plant Physiology* **129**: 112–121.

Kim JS, Kug JS, Jeong SJ, Huntzinger DN, Michalak AM, Schwalm CR, Wei Y, Schaefer K. 2017. Reduced North American terrestrial primary productivity linked to anomalous Arctic warming. *Nature Geoscience* **10**: 572–576.

Köhler IH, Ruiz-Vera UM, VanLoocke A, Thomey ML, Clemente T, Long SP, Ort DR, Bernacchi CJ. 2017. Expression of cyanobacterial FBP/SBPase in soybean prevents yield depression under future climate conditions. *Journal of Experimental Botany* **68**: 715–726.

Königer M, Delamaide JA, Marlow ED, Harris GC. 2008. *Arabidopsis thaliana* leaves with altered chloroplast numbers and chloroplast movement exhibit impaired adjustments to both low and high light. *Journal of Experimental Botany* **59**: 2285–2297.

Kromdijk J, Głowacka K, Leonelli L, Gabilly ST, Iwai M, Niyogi KK, Long SP. 2016. Improving photosynthesis and crop productivity by accelerating recovery from photoprotection. *Science* **354**: 857–861.

Kromdijk J, Głowacka K, Long SP. 2019. Predicting light-induced stomatal movements based on the redox state of plastoquinone: theory and validation. *Photosynthesis Research* **141**: 83–97.

Kromdijk J, Głowacka K, Long SP. 2020. Photosynthetic efficiency and mesophyll conductance are unaffected in *Arabidopsis thaliana* aquaporin knock-out lines. *Journal of Experimental Botany* **71**: 318–329.

Kromdijk J, Griffiths H, Schepers HE. 2010. Can the progressive increase of C_4 bundle sheath leakiness at low PFD be explained by incomplete suppression of photorespiration? *Plant, Cell & Environment* **33**: 1935–1948.

Le Quéré C, Raupach MR, Canadell JG, Marland G, Bopp L, Ciais P, Conway TJ, Doney SC, Feely RA, Foster P *et al.* 2009. Trends in the sources and sinks of carbon dioxide. *Nature Geoscience* **2**: 831–836.

Lichtenthaler HK. 1987. Chlorophylls and carotenoids: pigments of photosynthetic biomembranes. *Methods in Enzymology* **148**: 350–382.

Lobell DB, Roberts MJ, Schlenker W, Braun N, Little BB, Rejesus RM, Hammer GL. 2014. Greater sensitivity to drought accompanies maize yield increase in the U.S. Midwest. *Science* **344**: 515–519.

Long SP, Bernacchi CJ. 2003. Gas exchange measurements, what can they tell us about the underlying limitations to photosynthesis? Procedures and sources of error. *Journal of Experimental Botany* **54**: 2393–2401.

Long SP, Marshall-Colon A, Zhu XG. 2015. Meeting the global food demand of the future by engineering crop photosynthesis and yield potential. *Cell* **161**: 56–66.

López-Calcagno PE, Brown KL, Simkin AJ, Fisk SJ, Vialet-Chabrand S, Lawson T, Raines CA. 2020. Stimulating photosynthetic processes increases productivity and water-use efficiency in the field. *Nature Plants* **6**: 1054–1063.

Loriaux SD, Avenson TJ, Welles JM, Mcdermitt DK, Eckles RD, Riensche B, Genty B. 2013. Closing in on maximum yield of chlorophyll fluorescence using a single multiphase flash of sub-saturating intensity. *Plant, Cell & Environment* **36**: 1755–1770.

Okazaki K, Kabeya Y, Suzuki K, Mori T, Lchikawa T, Matsui M, Nakanishi H, Miyagishima S-Y. 2009. The plastid division1 and 2 components of the chloroplast division machinery determine the rate of chloroplast division in land plant cell differentiation. *Plant Cell* **21**: 1769–1780.

Osteryoung KW, Stokes KD, Rutherford SM, Percival AL, Lee WY. 1998. Chloroplast division in higher plants requires members of two functionally divergent gene families with hemology to bacterial *ftsZ. Plant Cell* **10**: 1991–2004.

Ray DK, Mueller ND, West PC, Foley JA. 2013. Yield trends are insufficient to double global crop production by 2050. *PLoS ONE* **8**: e66428.

Rosenthal DM, Locke AM, Khozaei M, Raines CA, Long SP, Ort DR. 2011. Over-expressing the C_3 photosynthesis cycle enzyme Sedoheptulose-1-7 Bisphosphatase improves photosynthetic carbon gain and yield under fully open air CO_2 fumigation (FACE). *BMC Plant Biology* **11**: 1–12.

Sharkey TD, Bernacchi CJ, Farquhar GD, Singsaas EL. 2007. Fitting photosynthetic carbon dioxide response curves for C_3 leaves. *Plant, Cell & Environment* **30**: 1035–1040.

Simkin AJ, López-Calcagno PE, Raines CA. 2019. Feeding the world: improving photosynthetic efficiency for sustainable crop production. *Journal of Experimental Botany* **70**: 1119–1140.

Slattery RA, Grennan AK, Sivaguru M, Sozzani R, Ort DR. 2016. Light sheet microscopy reveals more gradual light attenuation in light-green versus dark-green soybean leaves. *Journal of Experimental Botany* **67**: 4697–4709.

South PF, Cavanagh AP, Liu HW, Ort DR. 2019. Synthetic glycolate metabolism pathways stimulate crop growth and productivity in the field. *Science* **363**: eaat9077.

Tholen D, Zhu X-G. 2011. The mechanistic basis of internal conductance: a theoretical analysis of mesophyll cell photosynthesis and CO_2 diffusion. *Plant Physiology* **156**: 90–105.

Tilman D, Balzer C, Hill J, Befort BL. 2011. Global food demand and the sustainable intensification of agriculture. *Proceedings of the National Academy of Sciences, USA* **108**: 20260–20264.

Vogelmann TC, Evans JR. 2002. Profiles of light absorption and chlorophyll within spinach leaves from chlorophyll fluorescence. *Plant, Cell & Environment* **25**: 1313–1323.

Wada M, Kagawa T, Sato Y. 2003. Chloroplast movement. *Annual Review of Plant Biology* **54**: 455–468.

Wada M, Kong SG. 2019. Chloroplast actin filaments involved in chloroplast photorelocation movements. In: Sahi V, Baluška F, eds. *Plant cell monographs.* Cham, Switzerland: Springer, 37–48.

Weise SE, Carr DJ, Bourke AM, Hanson DT, Swarthout D, Sharkey TD. 2015. The arc mutants of Arabidopsis with fewer large chloroplasts have a lower mesophyll conductance. *Photosynthesis Research* **124**: 117–126.

Xiao Y, Sloan J, Hepworth C, Fradera-Soler M, Mathers A, Thorley R, Baillie A, Jones H, Chang T, Chen X *et al.* 2023. Defining the scope for altering rice leaf anatomy to improve photosynthesis: a modelling approach. *New Phytologist* **237**: 441–453.

Xiong D, Huang J, Peng S, Li Y. 2017. A few enlarged chloroplasts are less efficient in photosynthesis than a large population of small chloroplasts in *Arabidopsis thaliana. Scientific Reports* **7**: 1–12.

Yoon DK, Ishiyama K, Suganami M, Tazoe Y, Watanabe M, Imaruoka S, Ogura M, Ishida H, Suzuki Y, Obara M *et al.* 2020. Transgenic rice overproducing Rubisco exhibits increased yields with improved nitrogen-use efficiency in an experimental paddy field. *Nature Food* **1**: 134–139.

Supporting Information

Additional Supporting Information may be found online in the Supporting Information section at the end of the article.

Dataset S1 RT-qPCR cycle numbers.

Dataset S2 Chloroplast diameter lengths for glasshouse-grown plants.

Dataset S3 Chloroplast number per cell.

Dataset S4 Leaf width, palisade mesophyll cell size and number.

Dataset S5 Leaf anatomical parameters.

Dataset S6 Chloroplast movement characteristics.

Dataset S7 Pigment concentrations in glasshouse-grown leaves.

Dataset S8 Absorptance of light of glasshouse-grown leaves.

Dataset S9 Profiles of light absorption in leaves.

Dataset S10 Steady-state light (90% red and 10% blue) response curves for glasshouse-grown plants.

Dataset S11 Steady-state light (100%) response curves for glasshouse-grown plants.

Dataset S12 Fluctuating light (90% red and 10% blue) response curves for glasshouse-grown plants.

Dataset S13 CO_2 response curves for glasshouse-grown plants.

Dataset S14 Mesophyll conductance for glasshouse-grown plants.

Dataset S15 Chloroplast diameter lengths for field-grown plants.

Dataset S16 Pigment concentrations in field-grown leaves.

Dataset S17 Absorptance of light of field-grown leaves.

Dataset S18 Steady-state light-response curves for field-grown plants.

Dataset S19 CO_2 response curves for field-grown plants.

Dataset S20 Finale harvest field productivity experiment.

Fig. S1 Schematic representation of plasmids used in transformation.

Fig. S2 Schematic representation of field experimental design.

Fig. S3 Weather conditions during field experiment.

Fig. S4 Microscopic images of representative leaf mesophyll cells.

Fig. S5 Steady state of gas exchange and fluorescence parameters as a function of light (100% red) in glasshouse-grown plants.

Fig. S6 Response of gas exchange and fluorescence parameters to fluctuating light in glasshouse-grown plants.

Fig. S7 Chloroplast size and shape in the field-grown plants.

Fig. S8 Steady state of gas exchange and fluorescence parameters as a function of light in field-grown plants.

Fig. S9 Net CO_2 fixation rate as a function of intercellular CO_2 concentration in field-grown plants.

Fig. S10 Final sizes of the fractions of field-grown plants.

Methods S1 Measurements of leaf transmittance for chloroplast movement study.

Methods S2 Tissue fixation and slide preparation for the leaf anatomy study.

Methods S3 Quantification of photosynthesis-related pigments spectrophotometrically.

Methods S4 Light-sheet microscopy for estimation of light profiles within leaf.

Methods S5 Field experiment establishment and management.

Table S1 Primer sequences used in the study.

Table S2 Physiological parameters derived from the responses of gas exchange and fluorescence to absorbed light intensity for glasshouse- and field-grown plants.

Table S3 Inferred biochemical parameters derived from leaf photosynthetic CO_2 response curves of glasshouse- and field-grown plants.

Table S4 Quantification of photosynthesis-related pigments and absorptance of irradiance in field-grown plants.

Please note: Wiley is not responsible for the content or functionality of any Supporting Information supplied by the authors. Any queries (other than missing material) should be directed to the *New Phytologist* Central Office.